Superhydrophobic Surfaces as a Source of Airborne Singlet Oxygen Through Free Space for Photodynamic Therapy

David Aebisher,[1] Dorota Bartusik-Aebisher,[1] Sarah J. Belh,[2,3] Goutam Ghosh,[2,3] Andrés M. Durantini,[2,4] Yang Liu,[3,5] QianFeng Xu,[5] Alan M. Lyons,[3,5*] Alexander Greer[2,3*]

[1] Facility for Faculty, University of Rzeszów, 35-310, Rzeszów, Poland

[2] Department of Chemistry, Brooklyn College, City University of New York, Brooklyn, New York 10314, United States

[3] Ph.D. Program in Chemistry, Graduate Center of City University of New York, New York, New York 10016, United States

[4] IDAS-CONICET, Departamento de Química, Facultad de Ciencias Exactas, Físico-Químicas y Naturales, Universidad Nacional de Río Cuarto, Río Cuarto, Córdoba, Argentina

[5] Department of Chemistry, College of Staten Island, City University of New York, Staten Island, New York 10314, United States

Email addresses: alan.lyons@csi.cuny.edu; agreer@brooklyn.cuny.edu

Table of Contents Graphic

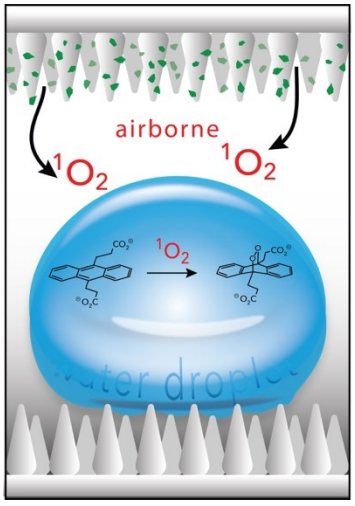

Keywords: singlet oxygen, physical quenching, superhydrophobic surface, liquid droplet, near IR detection, photodynamic therapy

Abstract

A superhydrophobic (SH) sandwich system has been developed to enable "contact-free" airborne singet oxygen ($^1O_2$) delivery to a water droplet. The contact-free feature means that the sensitizer is physically separated from the droplet, which presents opportunities for photodynamic therapy (PDT). Trapping of airborne $^1O_2$ in a H_2O droplet residing on a lower SH surface was monitored with 9,10-anthracene dipropionate dianion by varying distances to an upper $^1O_2$-generating surface. Short distances of 20 μm efficiently delivered airborne $^1O_2$ to the droplet in single-digit picomolar steady-state concentrations. Delivery decreases linearly with distance, but 50% of the $^1O_2$ steady-state concentration is trapped at a distance of 300 μm from the generating surface. The 1270 nm luminescence intensity was measured within the SH sandwich system confirming the presence of airborne $^1O_2$. Physical quenching of $^1O_2$ to ground-state $^3O_2$ by the water droplet itself; and both physical and chemical quenching of $^1O_2$ by the water droplet containing the trap 9,10-anthracene dipropionate dianion is observed. Unlike a majority of work in the field of PDT with dissolved sensitizers, where $^1O_2$ diffuses short (hundreds of nanometer) distances, we show the delivery of airborne $^1O_2$ via a superhydrophobic surface is effective through-air in tenths of millimeter distances to oxidize an organic compound in water. Our results provide not only potential relevance to PDT, but also surface bacterial inactivation processes.

Introduction

Several studies have focused on the generation of airborne singlet oxygen ($^1O_2$), including formation of $^1O_2$ at air/solid surfaces.[1-6] However, the literature is lacking with respect to airborne $^1O_2$ delivery without the actual contact of the $^1O_2$-generating surface with a second (distal) surface receiving $^1O_2$.

In this vein, we recently reported[7] the formation of airborne $^1O_2$ from the irradiation of sensitizer particles embedded in the plastron of a superhydrophobic surface (sensSH). In this earlier study, sensitizer coated polydimethylsiloxane (PDMS) posts were capped with PDMS coated with hydrophobic fumed silica nanoparticles, thereby preventing direct contact between the suspened water droplet and the sensitizer praticles in the plastron. Airborne $^1O_2$ was shown to transverse the plastron and reach a water droplet containing a water-soluble anthracene trapping agent (**1**) suspended on the SH surface. Since some sensitizer particles could be located within microns of the water droplet in this configuration, we wondered whether sensSH surfaces would be suited to deliver airborne $^1O_2$ over greater distances. However, no evidence yet exists for a "contact-free" delivery of $^1O_2$ between a sensSH surface and a water sample.

Thus, we wished to study the possible transit of airborne $^1O_2$, but with strictly no contact between the sensSH surface generating the $^1O_2$ and the water droplet recieving the $^1O_2$. We designed a sandwich structure that uses two separated superhydrophobic surfaces to enforce the delivery of airborne $^1O_2$ from an upper generating layer (sensSH) to a water droplet perched on a lower native SH surface containing no sensitizer particles (Figure 1). The sensitizer-containing surface does not contact the droplet and no sensitizer particles are transferred to the water. Reports exist on $^1O_2$ gas bubbles[8] and a SH surface with tips coated with silicone in contact with water[7,9] providing for minimal contact and sensitizer-free production of $^1O_2$. However, the

literature is devoid of measurements for the steady-state concentration and number of airborne $^1O_2$ molecules that diffuse outward from a SH surface over μm or mm distances.

The objective of the SH sandwich system developed here (Figure 2) is to determine how efficiently airborne $^1O_2$ migrates as a function of distance to a distal water droplet. Our hypothesis is that airborne $^1O_2$ will be detected tenths of millimeters beyond the generating surface. The steady-state concentration of $^1O_2$ and the number of $^1O_2$ molecules to reach the water surface were estimated. In this vein, the airborne $^1O_2$ luminescence intensity at 1270 nm was also examined to gauge the utility of $^1O_2$ delivery from a superhydrophobic surface. Information on such a *contact-free* SH surfaces adds key results to impact device development on the transport of airborne $^1O_2$ and deeper understanding of exposure of natural water droplets to reactive oxygen. The results also point to future use in PDT and biofilm erradication.

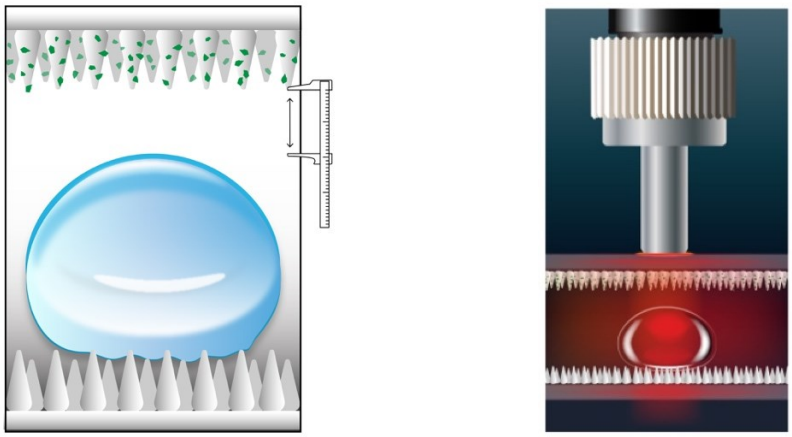

A B

Figure 1. Top-down approach of airborne $^1O_2$ to a water droplet. Schematics (A and B) are two representative images of the same sandwich device where airborne $^1O_2$ is delivered from an upper sensSH surface to a water droplet suspended on a second SH surface. The upper sensSH surface is embedded with sensitizer particles; the lower SH surface bears no sensitizer particles. Image A shows the measurement of the distance between the sensSH surface and droplet; image B shows the red diode laser placed directly above. The sandwich system allows for the contact-free $^1O_2$ delivery to the target H_2O droplet. A photograph of the sandwich device is also shown in Figure S1 (Supporting Information).

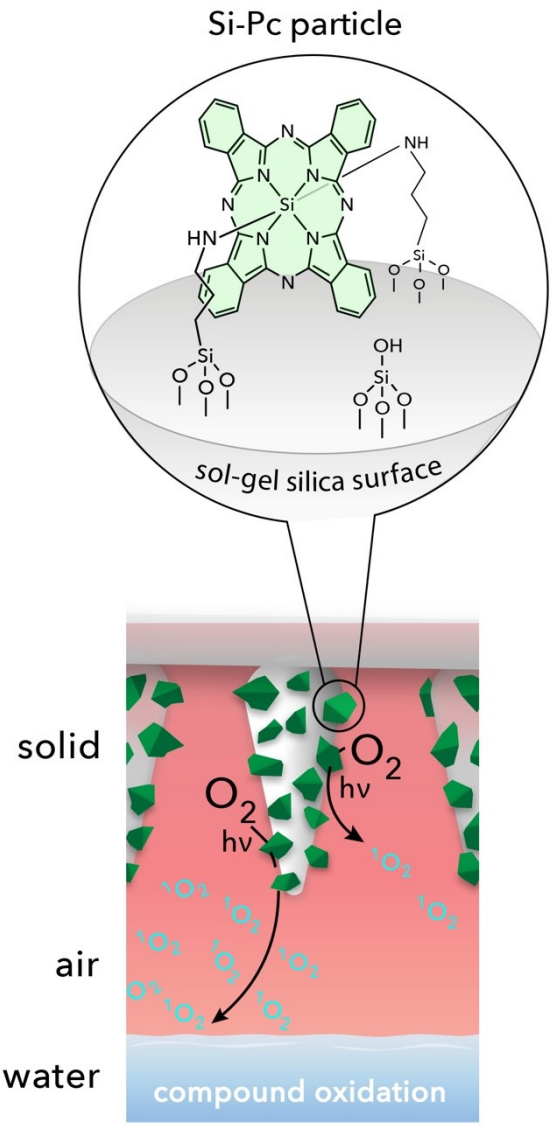

Figure 2. Schematic showing $^1O_2$ is delivered from Si-Pc particle embedded silica of the sensSH surface over an intervening air gap to water for compound oxidation. The shortest possible distance is from the post tips to the water droplet surface since the sensitizer particles have been dispersed evenly over the PDMS posts in the sensSH surface.

Experimental Section

Materials and Instrumentation. Silicon phthalocyanine dichloride (SiPcCl2), 3-aminopropyltriethoxysilane (ATPS), and 3-glycidyloxypropyl-trimethoxysilane (GPTMS) were purchased from Sigma Aldrich (Allentown, PA). Deionized water was purified using a U.S. Filter Corporation deionization system (Vineland, NJ). UV−visible spectra of the 9,10-anthracene dipropionate dianion **1** in H_2O were collected on an Agilent spectrophotometer. The concentration of O_2 in water was measured with a pO_2 Sens-Ion6 oxygen electrode (Hach Co., Loveland, CO), where calibrations were conducted in air-saturated water. Optical energy was delivered from a CW diode laser (669 nm output, 383 mW, Intense Ltd.).

Fabrication of Superhydrophobic Surfaces. The process for printing superhydrophobic surfaces was reported previously.[9,10] Briefly, PDMS posts, ~ 1 mm tall, were printed in 1 cm × 1 cm arays on 0.5 mm pitch on a glass slide. The silicon phthalocyanine (Si-Pc) glass particles (40-150 μm) were prepared as described previously.[8] The method for embedding of the Si-Pc particles into the SH surfaces was also reported previously.[7] An amount of sensitizer (8.3×10^{-8} mol) is contained within the 20 mg particles that are embedded into the sensSH surface. An average number of Si-Pc particles per SH post was found to be 70 ± 10 particles/post. Native SH surfaces containing no Si-Pc particles were also printed and used.

Apparatus. A 25-μL H_2O droplet was deposited onto a native lower SH surface using a calibrated pipet. The sensitizer-particle embedded superhydrophobic (sensSH) surface was placed face down above the droplet, at the fixed distances of: 20, 100, 200, 400 and 600 μm. These distances were measured in two ways: (1) with a caliper with 0.02 mm accuracy, and (2) with photographic images using ruler reference points and pixel size correlations.

Airborne $^1O_2$ Trapping. The sensSH surface was illuminated from the top with 669-nm light (383mW) passing through an FT-400-EMT optical fiber (Thorlabs, Newton NJ). The laserhead was positioned directly above a glass slide holding the sensSH surface face down. The formation of airborne $^1O_2$ was probed with anthracene **1** trapping in a 25-μL H_2O droplet sitting on the lower native SH surface. The concentration of **2** was determined with UV−vis by monitoring the disappearance of the absorption of **1** at λ = 378 nm at 10 min intervals for a total of 60 min. The concentration of **1** (0.2 mM) and pH of water (10.4) were chosen to readily detect **1** by UV−vis and solvate **1**, respectively. The anthracene **1** trap is not capable of photosensitizing $^1O_2$ with the longer wavelength (i.e., 669-nm) light that was used. The disappearance of **1** over the course of the reaction was first-order. The structure of anthracene endoperoxide **2** has been previously characterized on the basis of NMR and UV−vis spectroscopy.[7,12,13] Evidence for the stability of **2** for several days has been established, unlike naphthalene endoperoxides, and benzene endoperoxide, where the new C−O bonds are unstable and thereby prone to expulsion of O_2.[14,15] All experiments were carried out at ambient temperature (22 °C). We did not observe changes in droplet volume greater than 1 μL due to evaporation. The water temperature was increased minimally by only 0.5 °C over the 1 h irradiation period.

Direct Detection of Airborne $^1O_2$. The formation of airborne $^1O_2$ was demonstrated by monitoring its 1270 nm luminescence with a photomultiplier tube (H10330A-45, Hamamatsu Corp.). Before reaching the photomultiplier, the light emitting from the system was filtered through a 1250 nm long-pass and a 1270 nm band-pass filter (FWHM = 15 nm). The $^1O_2$ luminescence signals were registered on a 600 MHz oscilloscope. The samples were irradiated during 10 s to acquire 100 traces (10 Hz) that were averaged to obtain the luminescence intensity. A native SH surface with no sensitizer particles was used to measure the extent of

intensity enhancement due to noise and light scattering, but not due to airborne $^1O_2$. Datapoints for intensity vs time for each experimental condition were corrected by subtracting the intensities corresponding to noise and light scattering. To evaluate the presence of oxygen or nitrogen gas, they were directed at the sensSH surface with a feed tube connected to a gas tank. The gas flow rate was 130 ± 10 mL/min in both cases. Experiments with the SH sandwich system included the presence of a 25 μL H_2O droplet alone or the presence of a 25 μL H_2O droplet containing anthracene **1**.

Results and Discussion

Figures 1 and 2 show the sandwich SH system studied here which releases airborne $^1O_2$. The release of airborne $^1O_2$ occurs from the upper layer by photosensitization of $^3O_2$ on the embedded sensitizer particles (sensSH) with the subsequent migration of $^1O_2$ through the air gap to the 25-μL H_2O droplet containing anthracene **1**. The water droplet sits on a native SH surface which contains no sensitizer particles. As seen in Scheme 1 and described below, we find a distance-dependence in the $^1O_2$ migration with this sandwich SH system, which led us to elucidate the process, and is the topic of this paper.

Scheme 1. The SH sandwich system in which irradiation of the sensSH surface forms airborne $^1O_2$, which is quenched physically by the water droplet (k_d) and anthracene **1** (k_q), or where $^1O_2$ is trapped in a chemical reaction (k_r) thereby forming endoperoxide **2**.

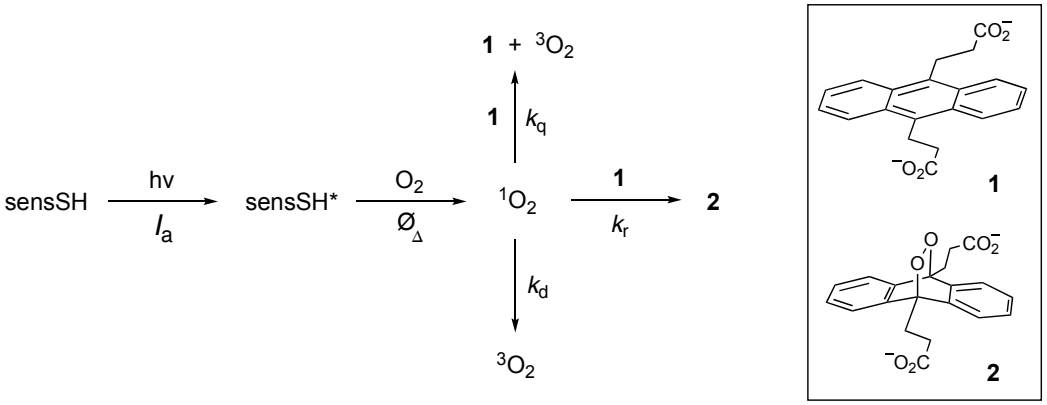

Kinetic Derivation. The SH sandwich is a 3-phase (solid-air-liquid) system. The first step in singlet oxygen formation is the activation of the solid sensitizer by visible light,

$$\text{sensSH} + h\nu\ (I_a) \rightarrow \text{sensSH}^* \tag{1}$$

where sensSH is the sensitizer particle embedded into the upper SH layer and I_a is the rate of absorption of 669-nm light by the sensitizer molecules in the upper SH layer (eq 1). When ground-state molecular oxygen (i.e., $^3O_2$) encounters the excited sensitizer, singlet oxygen ($^1O_2$) is formed and the sensitizer reverts to the ground state,

$$^3O_2 + \text{sensSH}^*\ (\Phi_\Delta) \rightarrow {}^1O_2 + \text{sensSH} \tag{2}$$

$$^1O_2\ (k_d) \rightarrow {}^3O_2 \tag{3}$$

where Φ_Δ is the quantum yield of $^1O_2$ production (eq 2). The $^1O_2$ formed is slowly quenched in air, but rapidly quenched in water to form ground-state $^3O_2$ (eq 3) where k_d is the rate constant for quenching of $^1O_2$ by water and air. The fewer molecules available to quench $^1O_2$ in the gas phase enables it to diffuse much greater distances compared to the solution phase.[8] In a water droplet, $^1O_2$ readily oxidizes **1** at the 9,10-position by a [4 + 2] reaction. The [4 + 2] reaction of $^1O_2$ is a common reaction in the field,[12,16-20] although it is usually monitored in the solution phase with a solvated sensitizer, which is unlike our SH sandwich system with a physically separated sensitizer. The physical quenching (k_q) and chemical quenching (k_r) of $^1O_2$ are shown in eqns 4 and 5.

$$^1O_2 + \mathbf{1}\ (k_q) \rightarrow {}^3O_2 + \mathbf{1} \quad (4)$$

$$^1O_2 + \mathbf{1}\ (k_r) \rightarrow \mathbf{2} \quad (5)$$

The use of **1** enables us to monitor the rate of $^1O_2$ capture in the water droplet to be estimated by the reduction of the concentration of **1**.

The rate law can be expressed as

$$\text{rate} = (k_r + k_q)[^1O_2][\mathbf{1}] \quad (6)$$

where k_r is the chemical quenching rate constant and k_q is the physical quenching rate constant of **1** with $^1O_2$. Instead of examining a second order reaction with the rate proportional to the two reactant concentrations, $[^1O_2]$ and [**1**], we simplify the analysis with the steady-state (ss) approximation

$$-d[\mathbf{1}]/dt = d[\mathbf{2}]/dt = (k_r + k_q)[^1O_2]_{ss}[\mathbf{1}] \quad (7)$$

$$-d[\mathbf{1}]/dt = (k_r\,[\mathbf{1}]) / (k_d + (k_r + k_q)[\mathbf{1}]) \quad (8)$$

where $[^1O_2]_{ss} = (-k_d - (k_r + k_q)\,[\mathbf{1}])^{-1}$ (Supporting Information, equation f) and k_q is taken to be zero since 9,10-disubstituted anthracene traps are known to be mainly chemical quenchers not physical quenchers of $^1O_2$.[15,19]

$$-d[\mathbf{1}]/dt = (k_r\,[\mathbf{1}]) / (k_d + k_r\,[\mathbf{1}]) \quad (9)$$

Under the condition, $k_r\,[\mathbf{1}] >> k_d$, the reaction is zero order. However, under the condition $k_d >> k_r\,[\mathbf{1}]$, the reaction is first order in the loss of **1**, which is useful for a kinetic analysis

$$-d[\mathbf{1}]/dt = k_r\,[^1O_2]_{ss}\,[\mathbf{1}] \quad (10)$$

$$-d[\mathbf{1}]/dt = k_{obs}\,[\mathbf{1}] \quad (11)$$

$$k_r\,[^1O_2]_{ss}\,[\mathbf{1}] = k_{obs}\,[\mathbf{1}] \quad (12)$$

enabling us to obtain k_{obs} from the slope of a plot of *ln* [**1**] vs time. The $[^1O_2]_{ss}$ can also be obtained from k_{obs}, where the reported value for the rate of $^1O_2$ reacting with **1** ($k_r = 8.2 \times 10^7$ $M^{-1}s^{-1}$)[12] is used to calculate the $^1O_2$ steady state concentration at each distance. The solution to eq 12 gives

$$k_{obs} / k_r = [^1O_2]_{ss} \quad (13)$$

The derivation of the equations for the steady-state approximation of $[^1O_2]_{ss}$ is shown in the Supporting Information.

Trapping Results. Table 1 shows how $^1O_2$ trapping depends on the setup of the SH sandwich system. Setup 1 (Figure 1B) used an irradiated sensitizer-embedded SH surface (sensSH) on the top and native SH surface on the bottom and irradiation from the top; setup 2 used the same surfaces (a sensSH surface on top and a native SH surface on the bottom) but with no irradiation; and setup 3 used native SH surfaces on both the top and bottom but with irradiation. Setups 2 and 3 did not lead to $^1O_2$ trapping in the H_2O droplet when sensitizer-free SH surfaces were used or in the absence of light.

In an additional control experiment, no decrease in **1** was detected when the sensSH surface was placed above the water droplet for 1 h, and then the droplet itself irradiated in the presence of **1**. Thus, sensitizer deposition into the water droplet was not observed, which we attribute to well-adhered silica Si-Pc particles to the SH surface and the covalent bonding of Si-Pc to the silica. Any loosly bound or unbound sensitizer particles were removed by forced air in the fabrication of the sensSH surface prior to use. Construction of calibration curves showed the UV−vis absorbance detection limit of the sensitizer is 1 μM and of anthracene **1** is 2-3 μM. Very low concentrations of sensitizer deposited into the water droplet may be unobservable directly by UV−vis, but by $^1O_2$ trapping using anthracene **1** it is observable to much lower concentrations. The reason is that one molecule of sensitizer can lead to an exponential amount of $^1O_2$ as it is a photocatalyst attesting to the fine quantitation ability of anthracene **1**. The capture of airborne $^1O_2$ in water droplets in setup 1 enabled an analysis of the kinetics of the process, as we will see next.

Observed Rate Constant (k_{obs}). The data show there is a light and sensitizer-surface dependence that leads to airborne $^1O_2$ trapping in the water droplet (Table 1, setup 1). Here, k_{obs} values were obtained as a function of distance between the sensSH surface and the top surface of

the droplet from the slopes of plots of first-order data (*ln* [**1**] vs time) for 10 min irradiation periods up to a total of 60 min. For illustration purposes, Figure S2 (Supporting Information) shows a plot of data for *ln* [**1**] vs time at the distance of 600 μm between the upper sensSH surface and the top of the water droplet. For a distance of 20 μm, k_{obs} was found to be 1.5×10^{-5} s^{-1} with an $R^2 = 0.999$. The magnitude of the slope is diminished when the distance between the sensSH surface and water droplet is increased. Upon increasing the distance between the sensSH and the water droplet by 30-fold from 20 μm to 600 μm, k_{obs} decreased by 78%. Next, we sought information on whether the steady-state concentration of singlet oxygen was substantially changed at various distances between the sensSH and the water droplet.

Table 1. Dependence of k_{obs} on the distance between the upper SH surface and the top of the 25-µL water droplet for three experimental configurations.

distance (µm) [a]	k_{obs} (s^{-1})		
	setup 1 [b] Sensitizer illumination	setup 2 [c] Sensitizer no illumination	setup 3 [d] No sensitizer illumination
20	1.5×10^{-5}	0	0
100	1.2×10^{-5}	0	0
200	1.0×10^{-5}	0	0
400	0.67×10^{-5}	0	0
600	0.33×10^{-5}	0	0

[a] Refers to the shortest possible distance from the sensSH tips to the top of the water droplet. In reality the distance is a range since the reach is an additional 1-mm to the valley floor of the plastron.

[b] Setup 1: Upper sensSH layer, lower native SH layer, irradiated with 669-nm light.

[c] Setup 2: Upper sensSH layer, lower native SH layer, no irradiation.

[d] Setup 3: Upper native layer, lower native SH layer, irradiated with 669-nm light.

Steady-state Concentration of Singlet Oxygen ($[^1O_2]_{ss}$). We calculated the steady-state concentration of $^1O_2$ in the sandwich SH system as a function of distance between the sensSH surface and the water droplet (Table 2). As we noted above, the $[^1O_2]_{ss}$ calculation is not affected by the quenching of H_2O due to pseudo-first order kinetic requirements being met for **1**.

Furthermore, the quenching of $^1O_2$ by dissolved oxygen ($^3O_2$) is a physical process.[21] The results show that the $^1O_2$ steady state concentrations within the surface layer of the droplet were calculated to be between hundreds of femtomolar (1.8×10^{-13} M) at short distances (e.g., 20 μm) and tens of femtomolar (4.0×10^{-14} M) at long distances (e.g., 600 μm).

The results argue for low steady-state concentrations of $^1O_2$. The $^1O_2$ steady-state concentrations measured in the SH sandwich (3-phase) system are similar to our previous SH system, in which sensitizer particles were in contact with water (i.e., a two-phase system) with ($7.0\text{-}8.5 \times 10^{-12}$ M).[7] Other two-phase systems, such as a solid natural organic matter/water system (1×10^{-12} M),[22,23] an aerosol/dissolved aromatic system (1×10^{-13} M), and a *meso*-tetra(*N*-methyl-4-pyridyl)porphine cation-exchanged (i.e., tightly adsorbed) onto porous Vycor glass in H_2O are also in the femtomolar region (1×10^{-14} M).[13]

The number of $^1O_2$ molecules that will transverse the air-water interface to react with the trap inside the droplet may be deduced from the data (Table 2). The number of $^1O_2$ molecules that are trapped by **1** in the droplet are 4.6-times higher at a distance of 20 μm compared to 600 μm. The last column in Table 2 shows the yield of trapped $^1O_2$ where we measured the decrease in **1**, which is assumed to result from reaction with singlet oxygen. The number of $^1O_2$ molecules reported in Table 2 reflect only those trapped by anthracene **1** in the droplet. A higher number of $^1O_2$ molecules would be expected to actually traverse the air gap of the device before reaching the droplet itself.

Table 2. Dependence of the steady-state concentration of $^1O_2$ with a distance between the sensSH surface and the water droplet.

distance (μm) [a]	$[^1O_2]_{ss}$, M	number of $^1O_2$ molecules [b]	concentration of anthracene 1 removed (M) [c]
20	1.8×10^{-13}	2.8×10^{6}	4.1×10^{-5}
100	1.5×10^{-13}	2.3×10^{6}	3.4×10^{-5}
200	1.2×10^{-13}	1.8×10^{6}	2.7×10^{-5}
400	8.1×10^{-14}	1.2×10^{6}	1.8×10^{-5}
600	4.0×10^{-14}	6.1×10^{5}	0.8×10^{-5}

[a] Refers to the shortest possible distance from the sensSH tips to the top of the water droplet. In reality the distance is a range since the reach is an additional 1-mm to the valley floor of the plastron.

[b] This is the number of $^1O_2$ molecules trapped, not the number in the steady-state.

[c] The disappearance of antracene **1** after a total of 60 min.

H_2O vs D_2O Droplet. In eq 9, the anthracene trapping agent **1** needs to be kept in low concentrations to calculate $[^1O_2]_{ss}$ and maintain first order in **1** while k_d needs to exceed k_T [**1**]. The singlet oxygen being quenched by H_2O in the reaction does not significantly affect the $[^1O_2]_{ss}$ measurements. The reason is that k_d for $^1O_2$ in H_2O (2.86×10^5 s^{-1})[24] is 17-fold greater than k_r [**1**] (1.64×10^4 s^{-1}) with an initial concentration for **1** of 200 μM. Thus, under our constant light intensity in H_2O, the disappearance of **1** fits first order kinetics. Theoretically, it

would have been favorable to reduce the concentration of **1** by a factor of 10, from 200 μM to 20 μM, thereby increasing the k_d : k_r [**1**] ratio from 1:17.4 to 1:174. This would slightly improve adherence of 1st order kinetics, but make absorbance measurements less accurate.

If D_2O was used in place of H_2O, the solvent quenching rate of $^1O_2$ would decrease substatially ($k_{d(D2O)}$ is 1.50×10^4 s^{-1} whereas $k_{d(H2O)}$ is 2.86×10^5 s^{-1}). In this case, the $[^1O_2]_{ss}'$ at a distance of 20 μm can be calculated (eq 14).

$$[^1O_2]_{ss}' = (k_{d(H2O)} / k_{d(D2O)}) [^1O_2]_{ss} = 3.4 \times 10^{-12} \quad (14)$$

However, in D_2O, $k_d \sim k_r$ [**1**] (when using 200 μM **1**), which would result in a deviation from first order kinetics, thereby providing an impetus for using H_2O instead of D_2O in the $[^1O_2]_{ss}$ measurements.

The lifetime of singlet oxygen is 20-fold greater in D_2O than H_2O, although pure D_2O is not better to use for these droplet experiments since estimation of the singlet oxygen concentration has the kinetic requirement for $k_d >> k_r$ [**1**] for the loss of **1** to be first order. Once $^1O_2$ reaches the H_2O droplet, it has a limited diffusion distance of ~150 nm, so that it does not penetrate deep. Singlet oxygen has a longer diffusion distance in D_2O of 2.8 μm. In both cases this is a minute fraction of the width of the droplet (~4 mm). Furthermore, within this fraction the rate of diffusion of **2** out and **1** in is thought to be sufficiently fast to maintain the concentration equilibrium throughout the droplet.

Distance Dependence. The relative k_{obs} values (Table 1 data, red curve) and the yield of trapped $^1O_2$ (Table 2 data, blue curve) are plotted as a function of sensSH-droplet distance (d) in Figure 3. In both cases, plots of relative k_{obs} and yield of **2** (yield of trapped $^1O_2$) vs time

descrease rapidly with distance. Clearly, the plots show a steep decrease in the concentration of singlet oxygen delivered to the droplet as the distance between the sensSH surface to the droplet increased. This leads us to propose that the transit of airborne $^1O_2$ is favored at <300 μm distances in the SH sandwich system. This compares to the approximate distance of 200 μm for airborne $^1O_2$ previously reported in a shallow vessel system.[6]

In the context of production of airborne $^1O_2$, there are caveats unique to the superhydrophobic surface. A relationship exists where the $^1O_2$ formed near tip ends reaches the water droplet to a greater extent than the $^1O_2$ formed deep in the plastron. The sensitizer particles at the tip will yield the shortest $^1O_2$ diffusion distance and thus less $^1O_2$ is wasted (i.e., decays to the ground state before encountering the droplet) as a consequence compared to particles residing for example 1-mm deep at the valley floor of the plastron. The current SH sandwich consists of a three-phase system where $^1O_2$ is generated on the PDMS posts, where most is delivered from the tip rather than deep in the plastron, as illustrated in Figure 2.

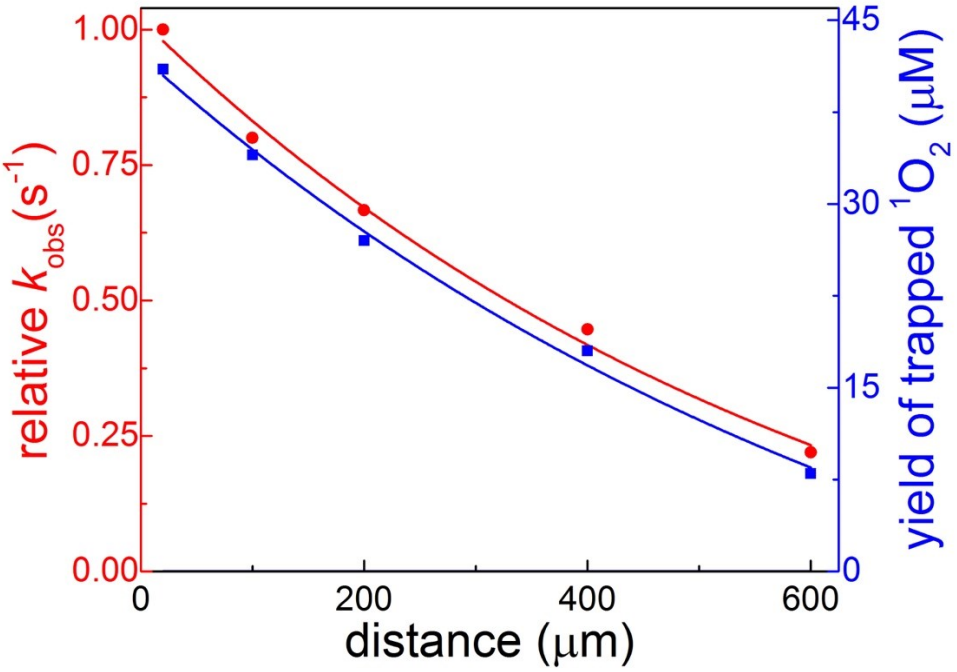

Figure 3. The dependence the reaction rate of $^1O_2$ with **1** (0.2 mM) and yield of trapped $^1O_2$ with increasing distance of the sensSH surface to the 25-μL H_2O droplet.

Luminescence from Airborne $^1O_2$. For evidence of the appearance of airborne $^1O_2$ in our SH sandwich system, luminescence measurements at 1270 nm were carried out. These experiments were done using the same system configuration described above, where the sensSH surface was irradiated from the top down. One hundred luminescence intensity vs time datapoints for various experimental conditions were collected and averaged to generate the data in Figure 4 (representative data collected over 4.5 ms are shown in Figure S2). The signal intensity in ambient conditions due to irradiation of the native SH surface alone is ~0.015 mV, which is attributed to background (Figure 4, 1st column). A 5-fold intensity enhancement was

observed upon replacement of the native SH surface by the sensSH surface alone with no native lower SH surface in the vicinity (Figure 4, 2nd column). Next, experiments were performed by flowing O_2 and N_2 gas at a rate of 130 mL/min onto the sensSH surface. A ~30% intensity increase (Figure 4, 3rd column) was observed when going from static air to flowing O_2 gas. However, replacement of O_2 by N_2 gas resulted in a 50% signal drop (Figure 4, 4th column). The SH sandwich system is an open system so that a complete drop in the signal is not expected. However, these data are consistent with a signal mainly from $^1O_2$ phosphorescence. No significant intensity decrease was detected when a native SH surface was placed 150 μm below the sensSH surface in the absence of a water droplet (Figure 4, 5th column). The sensitivity of the signal was tested by placing a 25 μL water droplet alone and a 200 μM solution of **1** on the lower native SH surface in the sandwich system (Figure 4, 6th and 7th columns). Here, the signal intensity reduced by 5% and 13% in comparison to the SH sandwich system alone. Carboxylic acid salts have been shown to reduce the surface tension of water.[25,26] Due to the droplet adopting a slightly flatter shape in the presence of **1** and NaOH, airborne $^1O_2$ arrives to a larger quenching area compared to a water droplet in their absence, which accounts for the 8% intensity increase in the former. Interestingly, no variation in the 1270 nm luminescence intensity was observed as a function of [**1**] concentrations at 0.2 mM, 10 mM, and 20 mM (Figure S3). This lack of sensitivity is attributed to two factors; the first one is the area of the sensSH surface is approximately 10 times larger than the surface area of the water droplet. With the droplet located in the center of the sandwich, the signal was mainly due to airborne $^1O_2$ produced on the SH surface above the droplet. Therefore, luminescence intensity is an average where ~90% of the signal is $^1O_2$ deactivated by air and only ~10% by the water droplet. The second factor is that

most of the $^1O_2$ that contacts the water droplet is physically quenched by water; (k_d) is 17-fold greater than the chemical quenching rate (k_r).

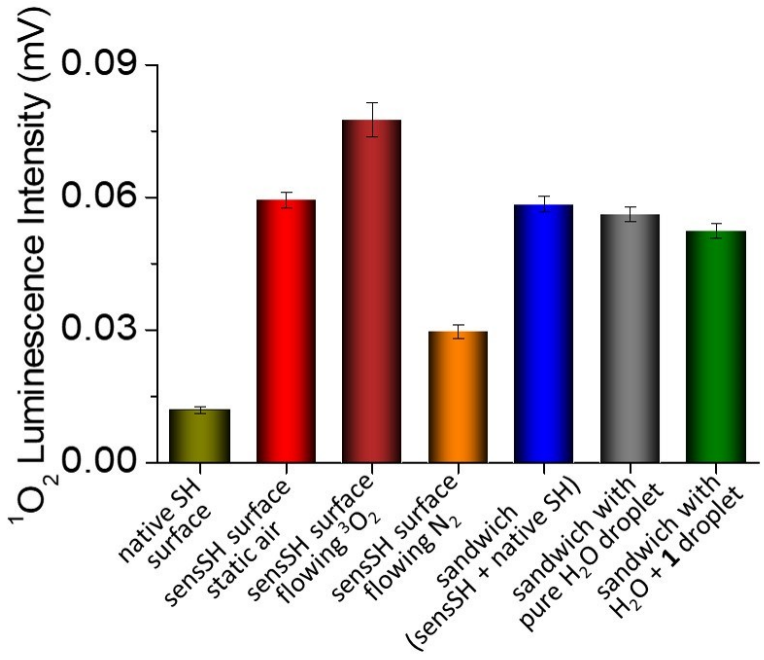

Figure 4. Luminescence intensity at 1270 nm for the (1st column) native SH surface containing no sensitizer particles; (2nd column) sensSH surface; (3rd column) sensSH surface with oxygen gas flowing at a rate of 130 mL/min; (4th column) sensSH surface with nitrogen gas flowing at a rate of 130 mL/min; (5th column) SH sandwich system with no water droplet; (6th column) SH sandwich system with the water droplet as physical quencher; (7th column) SH sandwich system using a water droplet with 0.2 mM of **1** as chemical quencher. The distance between the sensSH surface and the water droplet was 150 μm, and the system is open. Errors represents the standard deviation from duplicates experiments.

Summary

The data taken together provide evidence for the facile transit of airborne $^1O_2$ over a 20 μm distance, but this transport decreases rapidly with increasing distance. The data are also consistent with previous reports of airborne $^1O_2$ traveling tenths of millimeter distances to reach a liquid[6] or solid surface.[4] An important finding in our study is the steep drop in the number of singlet oxygen molecules that reach the water droplet depending on the distance separated from the upper $^1O_2$-generating SH surface. Furthermore, the luminescence data for $^1O_2$ in the air gap of the SH sandwich is consistent with physical and chemical quenching of $^1O_2$ with the droplet and with **1** within the droplet, respectively.

Conclusion

The SH sandwich system demonstrates a facile method for the delivery of $^1O_2$ in a contact-free manner. Because the sensitizer is isolated from the droplet, the sensitizer cannot participate in solution-phase photochemistry. In fact, some sensitizers are known to undergo electron-transfer reactions in the presence of O_2 in solution.[27,28] This leads to the formation of reactive intermediates and by-products, such as decomposed sensitizer molecules. Not only do our results show that $^1O_2$ can be delivered to a water droplet that is fully free from contact with the sensSH surface, they show a strong distance dependence correlation. Using a native SH surface to support the droplet on the lower portion of the sandwich structure proved highly advantageous because it facilitated recovery of the entire droplet without leaving any significant residue on the surface. Essentially no liquid remained on the native SH surface after it was removed with a pipette and so the concentration of **1** could be analyzed accurately.

Our work reveals key virtues of using airborne $^1O_2$ in a contact-free SH system. But an appreciation for airborne $^1O_2$ is only slowly increasing as a means to oxidize compounds[29] and inactive bacteria.[17,30] As of yet, there is only sparse mention of airborne $^1O_2$ in the organic chemistry and photobiology literature, which we feel can be greatly expanded on due to advantages the contact-free system provides. So far, Midden et al.[6] developed a shallow vessel system where $^1O_2$ gas reached a water layer to be quenched there. Majima et al.[4] studied airborne $^1O_2$ in a TiO_2 system where it reached a solid surface. A previous example of airborne $^1O_2$ toxicity is in planktonic[24] and biofilm conditions,[17] where facile inactivation took place and thus shows promise in the field of PDT. We propose that a contact-free SH surface may be an efficient means to inactivate bacteria. Importantly, $^1O_2$ toxicity can be realized in which the sensitizer does not contact the organism. In the current SH sandwich study, only the $^1O_2$ oxidation of anthracene **1** and luminescence of $^1O_2$ were examined.

Future work in the area would benefit from increased loading of the plastron with triplet sensitizer sites that may be used to increase the output of airborne $^1O_2$. Also, an assessment of singlet oxygen sensitizers (e.g., phthalocyanine, chlorin, metal-organic),[31,32] particle types (e.g., porous, non-porous, plasmonic nanoparticles),[33-37] and contributions from convection would also help in the optimization of SH surfaces for $^1O_2$ output. Such future studies are important for gaining an understanding of the delivery of airborne $^1O_2$ to infected biological sites.

Associated Content

Supporting Information. The Supporting Information is available free of charge on the ACS Publications website, which include a kinetic derivation, a photograph of the SH sandwich

system, a plot of *ln* [**1**] vs time, and plots of singlet oxygen luminescence intensities with various apparatus setups.

ORCID

David Aebisher: 0000-0002-2661-6570

Dorota Bartusik-Aebisher: 0000-0002-5557-5464

Andrés M. Durantini: 0000-0002-7898-4033

Alan M. Lyons: 0000-0003-4410-9756

Alexander Greer: 0000-0003-4444-9099

Acknowledgements

SJB, GG, AMD, and AG acknowledge support from the National Science Foundation (CHE-1856765) and PSC-CUNY. AMD also acknowledges support from a Fulbright-CONICET fellowship. YL acknowledges the support from the CUNY Graduate Center and the College of Staten Island. QX acknowledges support from CUNY Center for Advanced Technology funded by the NY's Empire State Development. We thank Leda Lee for help with the graphic arts and Prabhu Mohapatra for synthesizing the 9,10-anthracene dipropionate dianion.

References

(1) Walalawela, N.; Greer, A. "Remote Singlet Oxygen Delivery Strategies" *In:* Singlet Oxygen: Applications in Biosciences and Nanosciences. Nonell, S.; Flors, C. Eds, Royal Society of Chemistry, 2016, pp 335-354.

(2) Choudhury, R.; Greer, A. Synergism Between Airborne Singlet Oxygen and a Trisubstituted Olefin Sulfonate for the Inactivation of Bacteria. *Langmuir* **2014**, *30*, 3599-3605.

(3) Naito, K.; Tachikawa, T.; Fujitsuka, M.; Majima, T. Real-time Single-molecule Imaging of the Spatial and Temporal Distribution of Reactive Oxygen Species with Fluorescent Probes: Applications to TiO_2 Photocatalysts. *J. Phys. Chem. C* **2008**, *112*, 1048-1059.

(4) Naito, K.; Tachikawa, T.; Cui, S.-U.; Sugimoto, A.; Fujitsuka, M.; Majima, T. Single-Molecule Detection of Airborne Singlet Oxygen. *J. Am. Chem. Soc.* **2006**, *128*, 16430-16431.

(5) Eisenberg, W. C.; Taylor, K.; Murray, R. W. Gas-Phase Kinetics of the Reaction of Singlet Oxygen with Olefins at Atmospheric Pressure. *J. Phys. Chem.* **1986**, *90*, 1945-1948.

(6) Midden, W. R.; Wang, S. Y. Singlet Oxygen Generation for Solution Kinetics: Clean and Simple. *J. Am. Chem. Soc.* **1983**, *105*, 4129-4135.

(7) Aebisher, D.; Bartusik, D.; Liu, Y.; Zhao, Y.; Barahman, M.; Xu, Q.; Lyons, A. M.; Greer, A. Superhydrophobic Photosensitizers. Mechanistic Studies of $^1O_2$ Generation in the Plastron and Solid/Liquid Droplet Interface. *J. Am. Chem. Soc*. **2013**, *135*, 18990-18998.

(8) Bartusik, D.; Aebisher, D.; Ghafari, B.; Lyons, A. M.; Greer, A. Generating Singlet Oxygen Bubbles: A New Mechanism for Gas-Liquid Oxidations in Water. *Langmuir* **2012**, *28*, 3053-3060.

(9) Zhao, Y.; Liu, Y.; Xu, Q.; Barahman, M.; Bartusik, D.; Greer, A.; Lyons, A. M. Singlet Oxygen Generation on Porous Superhydrophobic Surfaces: Effect of Gas Flow and Sensitizer Wetting on Trapping Efficiency. *J. Phys. Chem. A* **2014**, *118*, 10364-10371.

(10) Barahman, M.; Lyons, A. M. Ratchetlike Slip Angle Anisotropy on Printed Superhydrophobic Surfaces. *Langmuir* **2011**, *27*, 9902-9909.

(11) Xu, Q.-F.; Liu, Y.; Lin, F.-J.; Mondal, B.; Lyons, A. M. Superhydrophobic TiO_2-polymer Nanocomposite Surface with UV-induced Reversible Wettability and Self-cleaning Properties. *ACS Appl. Mater. Interfaces* **2013**, *5*, 8915-8924.

(12) Lindig, B. A.; Rodgers, M. A. J.; Schaap, A. P. Determination of the Lifetime of Singlet Oxygen in D_2O Using 9,10-Anthracenedipropionic Acid, a Water-Soluble Probe. *J. Am. Chem. Soc.* **1980**, *102*, 5590-5593.

(13) Aebisher, D.; Zamadar, M.; Mahendran, A.; Ghosh, G.; McEntee, C.; Greer, A. Fiber-optic Singlet Oxygen [$^1O_2$ ($^1\Delta_g$)] Generator Device Serving as a Point Selective Sterilizer. *Photochem. Photobiol*. **2010**, *86*, 890-894.

(14) Zamadar, M.; Greer, A (2010) Singlet Oxygen as a Reagent in Organic Synthesis. In Handbook of Synthetic Photochemistry (Edited by A. Albini and M. Fagnoni), pp. 353-386. Wiley-VCH, Weinheim.

(15) Ghogare, A. A.; Greer, A. Using Singlet Oxygen to Synthesize Natural Products and Drugs. *Chem. Rev.* **2016**, *116*, 9994-10034

(16) Oliveira, M. S.; Severino, D.; Prado, F. M.; Angeli, J. P.; Motta, F. D.; Baptista, M. S.; Medeiros, M. H.; Mascio, P. Di. Singlet Molecular Oxygen Trapping by the Fluorescent Probe Diethyl-3,3'-(9,10-anthracenediyl)bisacrylate Synthesized by the Heck reaction. *Photochem. Photobiol. Sci.* **2011**, *10*, 1546-1555.

(17) Pushalkar, S.; Ghosh, G.; Xu, Q.; Liu, Y.; Ghogare, A. A.; Atem, C.; Greer, A.; Saxena, D.; Lyons, A. M. Superhydrophobic Photosensitizers: Airborne $^1O_2$ Killing of an *in-vitro* Oral Biofilm at the Plastron Interface. *ACS Appl. Mater. Interfaces* **2018**, *10*, 25819-25829.

(18) Brega, V.; Kanari, S. N.; Doherty, C. T.; Che, D.; Sharber, S. A.; Thomas, S. W. III. Spectroscopy and Reactivity of Dialkoxy Acenes. *Eur. J. Chem.* **2019**, 25, 10400-10407

(19) Fudickar, W.; Linker, T. Theoretical Insights into the Effect of Solvents on the [4 + 2] Cycloaddition of Singlet Oxygen to Substituted Anthracenes: A Change From a Stepwise Process to a Concerted Process. *J. Phys. Org. Chem.* **2019**, *32*, e3951.

(20) Kessel, D.; Price, M. Evaluation of Diethyl-3-3'-(9,10-anthracenediyl)bisacrylate as a Probe for Singlet Oxygen Formation During Photodynamic Therapy. *Photochem. Photobiol.* **2012**, *88*, 717-720.

(21) Schweitzer, C.; Schmidt, R. Physical Mechanisms of Generation and Deactivation of Singlet Oxygen. *Chem. Rev.* **2003**, *103*, 1685-1757

(22) Haag, W. R.; Hoigné, J. Singlet Oxygen in Surface Waters. 3. Photochemical Formation and Steady-state Concentrations in Various Types of Waters. *Environ. Sci. Technol.* **1986**, *20*, 341-348.

(23) Appiani, E.; McNeill, K. Photochemical Production of Singlet Oxygen from Particulate Organic Matter. *Environ. Sci. Technol.* **2015**, *49*, 3514−3522.

(24) Bartusik, D.; Aebisher, D.; Lyons, A. M.; Greer, A. Bacterial Inactivation by a Singlet Oxygen Bubbler: Identifying Factors Controlling the Toxicity of $^1O_2$ Bubbles. *Environ. Sci. Technol.* **2012**, *46*, 12098-12104.

(25) Badban, S.; Hyde, A. E.; Phan, C. M. Hydrophilicity of Nonanoic Acid and Its Conjugate Base at the Air/Water Interface. *ACS Omega* **2017**, *2*, 556-5573.

(26) Álvarez, E.; Vázquez, G.; Sánchez-Vilas, M.; Sanjurjo, B.; Navaza, J. M., Surface Tension of Organic Acids + Water Binary Mixtures from 20 °C to 50 °C. *J. Chem. Eng. Data* **1997**, *42*, 957-960.

(27) Baptista, M. S.; Cadet, J.; Mascio, P. Di.; Ghogare, A. A.; Greer, A.; Hamblin, M. R.; Lorente, C.; Nunez, S. C.; Ribeiro, M. S.; Thomas, A. H.; Vignoni, M.; Yoshimura, T. M. Type I and II Photosensitized Oxidation Reactions: Guidelines and Mechanistic Pathways. *Photochem. Photobiol.* **2017**, *93*, 912-919

(28) Clennan, E. L.; Pace, A. Advances in Singlet Oxygen Chemistry. *Tetrahedron* **2005**, *61*, 6665-6691.

(29) Malek, B.; Fang, W.; Abramova, I.; Walalawela, N.; Ghogare, A. A.; Greer, A. Ene Reactions of Singlet Oxygen at the Air-Water Interface. *J. Org. Chem.* **2016**, *81*, 6395-6401.

(30) Dahl, T. A.; Midden, W. R.; Hartman, P. E. Pure Singlet Oxygen Cytotoxicity for Bacteria. *Photochem. Photobiol.* **1987**, *46*, 345-352.

(31) Gollmer, A.; Felgenträger, A.; Maisch, T.; Flors, C. Real-time Imaging of Photodynamic Action in Bacteria. *J. Biophoton.* **2017**, *10*, 264-270.

(32) Dąbrowski, J. M.; Pucelik, B.; Regiel-Futyra, A.; Brindell, M.; Mazuryk, O.; Kyzioł, A.; Stochel, G.; Macyk, W.; Arnaut, L. G. Engineering of Relevant Photodynamic Processes Through Structural Modifications of Metallotetrapyrrolic Photosensitizers. *Coord. Chem. Rev.* **2016**, *325*, 67-101.

(33) Hackbarth**,** S.; Pfitzner, S.; Guo, L.; Ge, J.; Wang, P.; Röder, B. Singlet Oxygen Kinetics in Polymeric Photosensitizers. *J. Phys. Chem. C* **2018**, 122, 12071-12076

(34) Wang, S.; Gao, R.; Zhou, F.; Selke, M. Nanomaterials and Singlet Oxygen Photosensitizers: Potential Applications in Photodynamic Therapy. *J. Mater. Chem.* **2004**, *14*, 487-493.

(35) Macia, N.; Bresoli-Obach, R.; Nonell, S.; Heyne, B. Hybrid Silver Nanocubes for Improved Plasmon-Enhanced Singlet Oxygen Production and Inactivation of Bacteria. *J. Am. Chem. Soc.* **2019**, *141*, 684-692.

(36) Aebisher, D.; Azar, N. S.; Zamadar, M.; Gafney, H. D.; Gandra, N.; Gao, R.; Greer, A. Singlet Oxygen Chemistry in Water: A Porous Vycor Glass—Supported Photosensitizer. *J. Phys. Chem. B* **2008**, *112*, 1913-1917

(37) Cojocaru, B.; Laferrière, M.; Carbonell, E.; Parvulescu, V.; García, H.; Scaiano, J. C. Direct Time-resolved Detection of Singlet Oxygen in Zeolite-based Photocatalysts. *Langmuir*, **2008**, *24*, 4478-4481.